

FORMATION, TIDAL EVOLUTION AND HABITABILITY OF THE KEPLER-186 SYSTEM

EMELINE BOLMONT^{1,2}, SEAN N. RAYMOND^{1,2}, PHILIP VON PARIS^{3,+}, FRANCK SELSIS^{1,2}, FRANCK HERSANT^{1,2},
 ELISA V. QUINTANA^{4,5}, THOMAS BARCLAY^{5,6}

Draft version April 1, 2022

ABSTRACT

The Kepler-186 system consists of five planets orbiting an early-M dwarf. The planets have physical radii of 1.0-1.50 R_{\oplus} and orbital periods of 4 to 130 days. The 1.1 R_{\oplus} Kepler-186f with a period of 130 days is of particular interest. Its insolation of roughly 0.32 S_{\oplus} places it within the liquid water habitable zone. We present a multi-faceted study of the Kepler-186 system. First, we show that the distribution of planet masses can be roughly reproduced if the planets accreted from a high-surface density disk presumably sculpted by an earlier phase of migration. However, our simulations predict the existence of 1-2 undetected planets between planets e and f. Next, we present a dynamical analysis of the system including the effect of tides. The timescale for tidal evolution is short enough that the four inner planets must have small obliquities and near-synchronous rotation rates. Tidal evolution of Kepler-186f is slow enough that its current spin state depends on a combination of its dissipation rate and the stellar age. Finally, we study the habitability of Kepler-186f with a 1-D climate model. The planet's surface temperature can be raised above 273 K with 0.5-5 bars of CO₂, depending on the amount of N₂ present. Kepler-186f represents a case study of an Earth-sized planet in the cooler regions of the habitable zone of a cool star.

Subject headings: planetary systems; stars: individual (Kepler-186, KIC 8120608), methods: N-body simulations

1. INTRODUCTION

The *Kepler* mission (Borucki et al. 2010) has made key discoveries on the road to finding Earth-like planets (e.g., Batalha et al. 2011; Borucki et al. 2012; Fressin et al. 2012; Borucki et al. 2013). The recent detection of an Earth-sized planet in the habitable zone of an M-star (i.e., the Kepler-186 system, Quintana et al. 2014) brings us a step closer to finding a true Earth twin.

The Kepler-186 planetary system hosts 5 known planets including Kepler-186f, an Earth-sized planet in the habitable zone (Selsis et al. 2007; Kopparapu et al. 2013). Figure 1 shows a comparison between the Kepler-186 system, the solar system, and two other systems with potentially habitable planets: Kepler-62 (Borucki et al. 2013) and GJ 581 (Udry et al. 2007; Mayor et al. 2009). Climate models have shown that GJ 581d, a super-Earth near the outer edge of the habitable zone of its host M star, could sustain surface liquid water (e.g., Wordsworth et al. 2010). Kepler-186f receives a comparable or perhaps slightly higher stellar flux than GJ 581, placing it

more comfortably within the habitable zone.

We present a three-pronged study of the Kepler-186 system. We first try to reproduce the orbital architecture of the system using simple accretion simulations (Section 2). We show that certain features of the system – such as the large gap between planets e and f – are hard to explain. We next briefly discuss the long-term dynamical stability of the system (Section 3). In Section 4 we study the long-term dynamical, tidal and spin evolution of the system. We use both simple tidal models and N-body simulations that include both tides and general relativity. Next we study the atmospheric conditions needed to bring Kepler-186f's surface temperature into the liquid water range (Section 5). We discuss our findings and conclude in Section 6.

The stellar properties and planets' parameter given in Quintana et al. (2014) are the median values of each corresponding probability density. However, the median values are not intended to be self consistent (for example, the relation between density, radius and mass of the star is not respected). In order to study the dynamical evolution of the system and its habitability, we need a set of consistent parameters. There are two ways of obtaining a consistent set of values. They define what we call set \mathcal{A} and set \mathcal{B} :

- Set \mathcal{A} : The stellar properties are chosen to match the point estimate transit model obtained by doing MCMC realizations;
- Set \mathcal{B} : The transit model is chosen to match the point estimate stellar properties obtained by doing MCMC realizations. The stellar properties of this set correspond to those of table S1 in Quintana et al. (2014).

The stellar mass is 0.5359 M_{\odot} in set \mathcal{A} and 0.478 M_{\odot} in set \mathcal{B} . This produces different values for the plan-

¹ Univ. Bordeaux, Laboratoire d'Astrophysique de Bordeaux, UMR 5804, F-33270, Floirac, France

² CNRS, Laboratoire d'Astrophysique de Bordeaux, UMR 5804, F-33270, Floirac, France

³ Institut für Planetenforschung, Deutsches Zentrum für Luft- und Raumfahrt (DLR), Rutherfordstr. 2, 12489 Berlin, Germany

⁴ SETI Institute, 189 Bernardo Ave, Suite 100, Mountain View, CA 94043, USA

⁵ NASA Ames Research Center, Moffett Field, CA 94035

⁶ Bay Area Environmental Research Institute/NASA Ames Research Center, Moffett Field, CA 94035, USA

⁺ now at: Univ. Bordeaux, Laboratoire d'Astrophysique de Bordeaux, UMR 5804, F-33270, Floirac, France and CNRS, Laboratoire d'Astrophysique de Bordeaux, UMR 5804, F-33270, Floirac, France

* To whom correspondence should be addressed. email: bolmont@obs.u-bordeaux1.fr

ets’ semi-major axes and insolarations. The same is true for planetary radii, as these are derived from the detected transit depth and the stellar radius. We expect the real parameters of the system to be within the range of sets \mathcal{A} and \mathcal{B} , so we performed dynamical simulations for these both sets. Note that in Quintana et al. (2014), semi-major axes are not chosen to match the derived stellar properties, but are rather determined by the transit model only, a different approach than chosen here (where the independent stellar and transit models are forced to match).

All five planets in the Kepler-186 system have radii between 1.0 and 1.5 R_{\oplus} . Given that low-density, gas-dominated planets tend to be larger than $1.5 - 2R_{\oplus}$ (Weiss et al. 2013a; Weiss & Marcy 2014; Lopez & Fortney 2013; Jontof-Hutter et al. 2014; Marcy et al. 2014b,a), all five Kepler-186 planets are probably rocky or at least solid. The planets’ masses have not been constrained with radial velocity or transit timing measurements (Quintana et al. 2014). Table 3 shows the range of plausible planetary masses assuming a range of compositions: 100% ice, 50% ice/ 50% rock, Earth-like composition, and 100% iron (following Fortney et al. 2007).

2. FORMATION

2.1. Formation

At least six candidate mechanisms have been proposed to explain the origin of close-in low-mass planets (Raymond et al. 2008, 2013). These mechanisms can in theory be distinguished using two observable quantities: the inner planetary system architecture and the mean planet density. Given current constraints, the two leading candidates are the collisional growth of a population of inward-migrating planetary embryos (Terquem & Papaloizou 2007a; Cossou et al. 2014) and in-situ accretion of a population of close-in planetary embryos (Raymond et al. 2008; Chiang & Laughlin 2013). These two mechanisms might work in tandem, with an early phase of inward migration followed by a later phase of collisions (Hansen & Murray 2012; Raymond et al. 2013).

A problem with the in-situ accretion model is that it requires very massive disks close to their stars. For the observed systems of hot Super Earths to have accreted locally, the typical inner disk must be far more massive than that suggested by sub-mm observations of outer disks (Raymond et al. 2008). In addition, the inner disk must follow a steeper surface profile. Whereas outer disks are observed to follow $r^{-(0.5-1)}$ radial surface density profiles (Mundy et al. 2000; Andrews & Williams 2007b), a “minimum-mass extrasolar nebula” would need to follow an $r^{-1.6}$ profile (Chiang & Laughlin 2013). In fact, the minimum-mass disks inferred from the observed systems of hot Super Earths span a wide range of disk profiles, from $r^{0.5}$ to r^{-3} (Raymond & Cossou 2014). This is in conflict with all known disk theories. The concept of a universal disk is not viable.

2.2. Minimum-mass disk analysis

We performed a simple minimum-mass experiment on this system. We first calculated mass estimates for the planets. As a baseline we assumed that their bulk compositions are the same as Earth’s and used a corresponding mass-radius relation (following Valencia

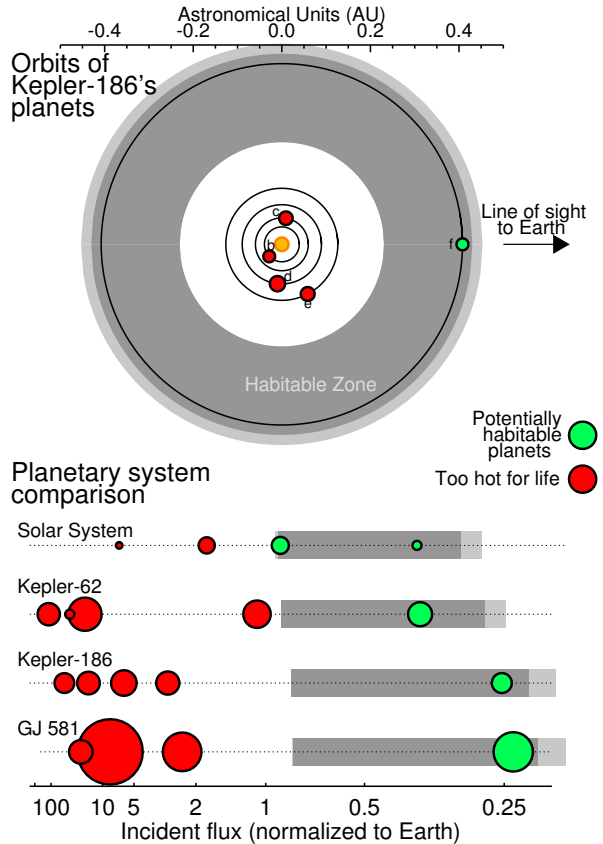


FIG. 1.— Orbital configuration of the Kepler-186 system. The top part shows a top-down view of the system, assuming orbits from set \mathcal{A} . The habitable zone boundaries are from Kopparapu et al. (2013): the inner boundaries are the moist/runaway greenhouse limits and the outer boundaries are the maximum greenhouse and early Mars limits. The sizes of the symbols are not to scale with the planetary orbits. The bottom part of the plot shows a comparison between four different planetary systems that contain planets in the habitable zone: the Solar System, Kepler-62 (Borucki et al. 2013), Kepler-186 (Quintana et al. 2014), and GJ 581 (Udry et al. 2007; Mayor et al. 2009). Given the consistent insolation scaling, the x-axis is linear in orbital distance but the scale is different for each system. The planets’ relative sizes are correct, although for GJ 581 the planetary radii were calculated as $R = [M \sin(i)]^{2.06}$, following Lissauer et al. (2011).

et al. 2006) whereby $M \propto R^{3.7}$. We also tested other observationally-derived mass-radius relations: $M \propto R^{2.06}$ (Lissauer et al. 2011) and the empirical, flux-dependent relation from Weiss et al. (2013b). We spread the planets’ masses into concentric annuli with boundaries at the geometric means between orbital radii and fit a simple power law.

Figure 2 shows the outcome of this experiment. The fiducial best fit was a very steep profile: $\Sigma(r) \propto r^{-2.64}$. Using only the four innermost planets in the fit – and testing different mass-radius relations – the slope of the surface density profile remained in a well-confined range: $\Sigma(r) \propto r^{-(2.5-2.7)}$. While the four inner planets are in a “packed” orbital configuration, there is a large gap between planets e and f . It is possible that an additional, as-yet undetected planet could exist within this gap (see below). We therefore repeated the minimum-mass disk experiment using just the four inner planets. This yielded a flatter profile with $\Sigma(r) \propto r^{-1.47}$. We repeated this experiment with both sets \mathcal{A} and \mathcal{B} and

TABLE 1
STELLAR PROPERTIES.

	Mass (M_{\odot})	Radius (R_{\odot})	T_{eff} (K)	L_{\star}/L_{\odot}
Set \mathcal{A}	0.536	0.5138	3747	0.0468
Set \mathcal{B}^a	0.478	0.4720	3788	0.0412

^aFrom Table S1 of Quintana et al. (2014)TABLE 2
PLANETARY PHYSICAL PARAMETERS.

		Kepler-186b	Kepler-186c	Kepler-186d	Kepler-186e	Kepler-186f
Period (days) ^a		3.887	7.267	13.34	22.41	129.9
Semimajor axis (AU)	Set \mathcal{A}	0.0393	0.0596	0.0894	0.1264	0.4078
	Set \mathcal{B}	0.0378	0.0574	0.0861	0.1216	0.3926
Radius (R_{\oplus})	Set \mathcal{A}	1.16	1.33	1.50	1.36	1.17
	Set \mathcal{B}	1.08	1.25	1.39	1.33	1.13

^aFrom Table S2 of Quintana et al. (2014), roundedTABLE 3
RANGE OF PLAUSIBLE PLANET MASSES (IN M_{\oplus}) USING FORMULAS FROM FORTNEY ET AL. (2007) FOR SET \mathcal{B} .

	Pure Ice	50% ice-rock	Earth-like	Pure Iron
Planet b	0.29	0.48	1.32	3.36
Planet c	0.46	0.77	2.27	6.30
Planet d	0.65	1.10	3.45	10.2
Planet e	0.56	0.95	2.89	8.32
Planet f	0.33	0.55	1.55	4.06

found slopes that were the same to within ± 0.01 . The rest of the analysis in this section uses set \mathcal{B} as comparison sample.

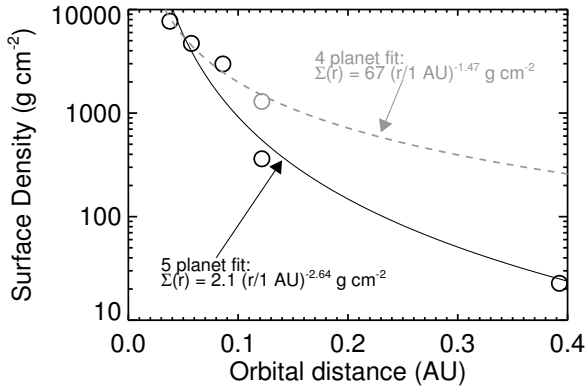


FIG. 2.— “Minimum-mass solar nebula”-type fit to the Kepler-186 system. The symbols were calculated assuming an Earth-like composition for all of the planets. The solid curve is the fiducial best fit. The other curves are best fits with modified assumptions regarding the planets’ masses (dotted curve) and using only the four inner planets in the fit (gray dashed curve). Although this plot shows fits for set \mathcal{B} , the inferred minimum-mass disks were almost identical using set \mathcal{A} .

The steep surface density profile from Fig 2 can be interpreted as the initial conditions for the final stage of planetary formation in this system. This is likely *after* a phase of inward migration of solids. Inward migration could potentially occur when objects are boulder-sized

or smaller (Weidenschilling 1977; Boley & Ford 2013; Chatterjee & Tan 2014) or when they are \sim Mars-sized or larger (Goldreich & Tremaine 1980; Ward 1997). Viscous disk models predict $r^{-(0.5-1)}$ profiles like the observed outer disks (Williams & Cieza 2011), so it is hard to imagine that such a steep profile could truly represent the state of the gaseous protoplanetary disk. Rather, the inner parts of the disk may have been enhanced by a prolonged phase of inward migration of Mars-sized or larger planetary embryos (Terquem & Papaloizou 2007a; Hansen & Murray 2012; Cossou et al. 2014). Migration tends to produce systems of planets in chains of mean motion resonances (e.g. Ogihara & Ida 2009; Cossou et al. 2013). Later dynamical evolution – possibly including a phase of giant impacts – can extract the planets from resonance (Terquem & Papaloizou 2007a; Cossou et al. 2014).

2.3. Accretion simulations

We attempted to reproduce the Kepler-186 system numerically. We started from the minimum-mass disks in Fig. 2 that were presumably already sculpted by migration, with surface density profiles $\Sigma \propto r^{-2.64}$ and $\Sigma \propto r^{-1.47}$. We performed two sets of N-body simulations of late-stage accretion of planetary embryos. Our initial conditions consisted of populations of 40 planetary embryos and 400 planetesimals spread between 0.02-0.04 and 0.5 AU. The total mass in solids was $15M_{\oplus}$. Embryos were given physical densities of 3 g/cm^3 . The embryos’ initial inclinations were randomly chosen between zero and 0.1° . Each system was integrated with the *Mercury* hybrid integrator (Chambers 1999) for 10 Myr using a 0.2

day timestep. Collisions were treated as perfect mergers and gas effects were not included. Given the short lifetimes of gaseous protoplanetary disks (Haisch et al. 2001; Hillenbrand 2008), the assumption of a gas-free environment may not be realistic. However, this could be justified if we assume that our initial conditions were sculpted by an earlier phase of migration and thus represent the state of the disk just after the dissipation of the gaseous disk. In that case, our choices of embryo and planetesimal masses have little effect on the outcome (Kokubo et al. 2006).

Figure 3 shows the evolution of a simulation in an $r^{-2.64}$ disk that formed six planets interior to 0.5 AU. Accretion was fast and proceeded as a wave sweeping outward. The outward-sweeping is caused by the radial dependence of the eccentricity excitation and encounter timescales. Accretion was mostly finished interior to 0.1 AU within 10^5 years and is complete throughout the disk by 1-10 Myr. Three planets formed between 0.03 and 0.11 AU, the range occupied by four planets in the Kepler-186 system. The simulation produced three additional planets including a reasonable analog to Kepler-186f at 0.31 AU. One of the extra planets was located at 0.19 AU, in the empty gap between planets *e* and *f*.

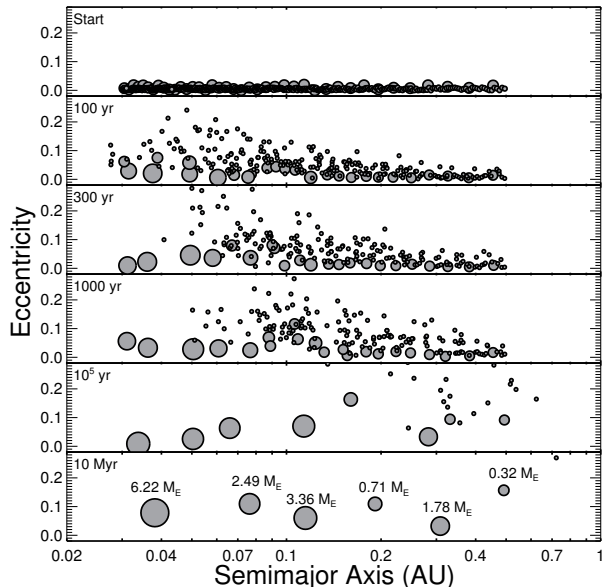


FIG. 3.— Evolution of a simulation of terrestrial accretion. Each circle corresponds to a growing planetary embryo or planetesimal with radius $R \propto M^{0.27}$ (Valencia et al. 2006, not to scale on the x axis). The masses of the final planets are labeled in the last panel.

Figure 4 shows the mass vs. orbital radius distribution for the N-body simulations, compared with the actual Kepler-186 system. Radii of the simulated planets were calculated assuming an Earth-like composition ($R \propto M^{0.27}$ (Valencia et al. 2006)). The distributions of accreted planets clearly retain a “memory” of their initial disk profiles (Raymond et al. 2005a). The planets that formed in disks with a steeper ($r^{-2.64}$) surface density profile were more massive close in and smaller farther out compared with the planets formed within the shallower ($r^{-1.47}$) profile.

The disk with a shallower ($r^{-1.47}$) profile provides a

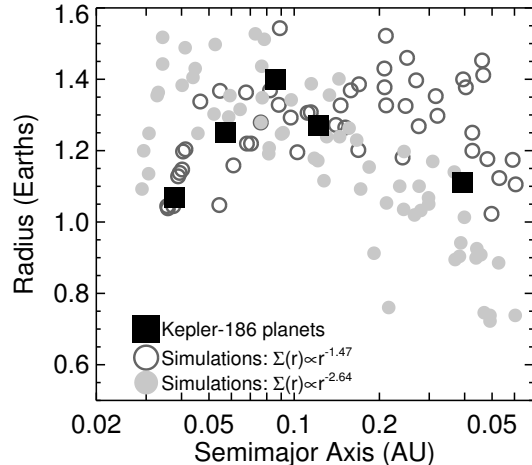


FIG. 4.— Size vs orbital radius for the Kepler-186 system (large black squares) compared with different suites of N-body simulations in disks with different properties (symbols).

better fit to the inner parts of the system’s mass distribution. However, neither set of simulations does a good job of fitting the outer parts of the system. Planet *f*’s size is systematically underestimated in simulations with a steeper ($r^{-2.64}$) disk and systematically overestimated in simulations with a flatter ($r^{-1.47}$) disk. The two innermost planets’ sizes are also systematically overestimated in the steeper disk. Given that the flatter disk profile was built using just the four inner planets, it is reassuring that the planets that formed in such a disk do indeed roughly match the mass distribution within ~ 0.1 AU. The fact that more distant planets are more massive than the real planet *f* is not surprising.

The inclinations of the simulated planets were too large to be consistent with the true system. Of particular importance is the mutual inclination between two planets’ orbits Φ_{12} , calculated as:

$$\cos \Phi_{12} = \cos i_1 \cos i_2 + \sin i_1 \sin i_2 \cos(\Omega_1 - \Omega_2), \quad (1)$$

where i denotes each planet’s inclination and Ω is the longitude of ascending node.

Figure 5 shows the mutual inclinations of the systems relative to the closest analog of planet *f* in each simulation. Planet *f* analogs were simply the planets closest to the true planet *f*’s orbital radius. In the shaded area of Fig. 5 a planet’s inclination relative to the plane of planet *f*’s orbit is smaller than the angular size of the star. This means that, if planet *f* transits, so too will the other planet. Above the shaded region a planet is statistically unlikely to transit if planet *f* transits. For most observing geometries the planet will not cross the stellar surface.

It is clear from Fig. 5 that the simulations produce systems that are too dynamically hot. The mutual inclinations between planets are too large for five planets to be observed in transit (Raymond & Cossou 2014). The observed multiple-planet systems are inferred to typically have mutual inclinations of not more than a few degrees (Fang & Margot 2012; Tremaine & Dong 2012). Additional mechanisms such as tidal damping have been invoked to decrease mutual inclinations on long timescales (see Hansen & Murray 2013). Nonethe-

less, these overly large mutual inclinations could be counted as an additional strike against the in-situ formation mechanism for hot super-Earths.

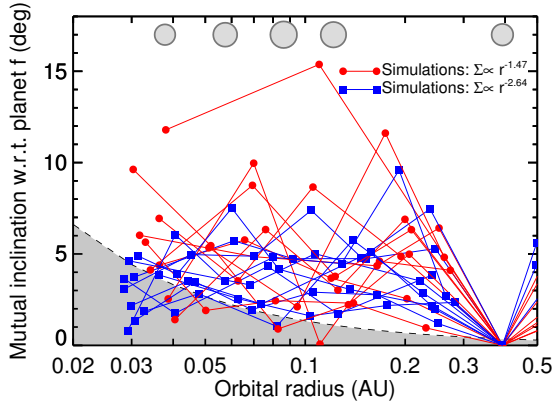


FIG. 5.— Mutual inclinations relative to analogs of planet f in the simulated systems. Orbital radii were scaled such that the planet f analogs were located at the correct distance. The planets’ actual positions (set \mathcal{B}) are shown by the gray symbols at the top of the plot.

2.4. A missing planet between planets e and f?

The most glaring inconsistency between the simulations and the Kepler-186 system is that the simulations form too many planets (Figure 6). Our simulations produced 3-8 planets interior to 0.5 AU. Most (12/20) simulations produced 6 or more planets. In all simulations at least one planet formed between the orbits of known planets e and f, in the range 0.15-0.4 AU. In the simulations that formed 5 planets, the inner parts of the systems tended to have less tightly-packed orbital configurations than the real one. But the outer parts of these systems (from 0.1-0.4 AU) were more packed.

Figure 7 shows the spacing of adjacent planets in the simulated systems compared with the real one. The bulk of simulated planet pairs have period ratios P_2/P_1 between 1.5 and 2.5. The planets that formed in the steep ($r^{-2.64}$) disk are more tightly-packed, with median period ratio of $P_2/P_1 = 2.0$ compared with a median of $P_2/P_1 = 2.24$ for the planets that formed in the shallow ($r^{-1.47}$) disk. We attribute this to the larger amount of mass in the inner parts of the disk, which tends to accelerate accretion at early times while there is strong dynamical friction (see Raymond et al. 2005b). In the shallow disk accretion is slower close-in and the late phases of accretion have less dynamical friction.

For the four inner planets in the Kepler-186 system, the period ratios of adjacent planets P_2/P_1 are confined between 1.6 and 1.9. Farther out is a wide gap: planets e and f have $P_2/P_1 = 5.82$. These two planets are more widely-separated than any planet pair in the simulations (except for one exceptional simulation – simulation 6 in Fig. 6 – that only formed three, very widely-spaced planets). Apart from that case, the most widely-separated simulated planet pairs had $P_2/P_1 \approx 3$. One or even two additional planets could comfortably fit between the orbits of planets e and f. All of the simulations contained such planet(s).

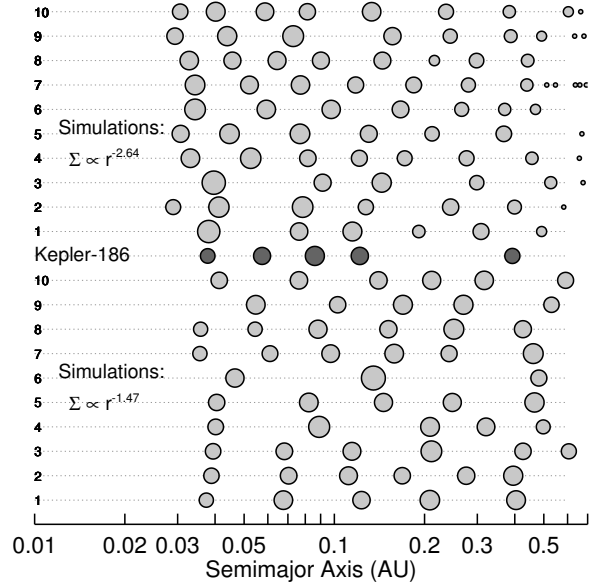


FIG. 6.— Final state of the 20 simulated systems compared with the actual one. The size of each simulated planet was scaled assuming a rocky composition.

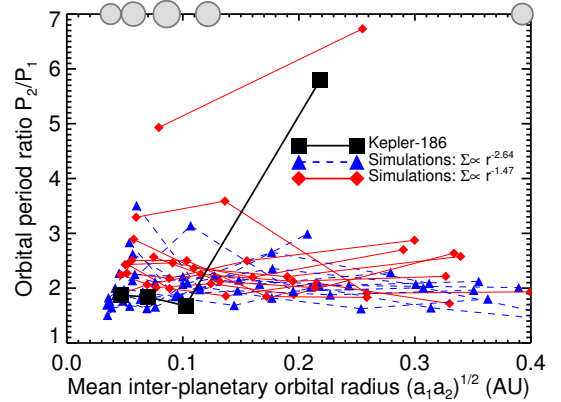


FIG. 7.— Orbital period ratio of pairs of adjacent planets as a function of the two planets’ (geometric) mean position. The different sets of simulations are shown with the grey symbols, and the real system with the large black squares. Each system is connected. The real system is indicated at the top of the plot.

Could an additional planet exist between planets e and f but not transit? For that to be the case, that planet would need to have an inclination of at least 1-2 degrees with respect to the common plane of the other planets (see section 4.2). A collision or scattering event after the dissipation of the gaseous disk could produce such an inclination. It would then be a simple coincidence that planet f’s orbit is aligned with the inner ones whereas this extra planet’s is not. Or, if this extra planet is somewhat lower-mass than the other planets then its secular oscillations in inclination could simply reach a higher amplitude than the other planets, decreasing the probability of observing it in common transit with the other planets.

On the other hand, what conditions of formation would be required for there *not* to be another planet in between planets e and f? As shown in Fig. 7, in-situ accretion does not produce large gaps between planets. An alternative

is that the planets formed farther out in the disk and migrated inward (Terquem & Papaloizou 2007b; Cossou et al. 2014). Structure within the disk – such as an opacity transition – can provide a mechanism to stop inward migration at different, or at least time-dependent, orbital radii (e.g. Masset et al. 2006; Bitsch et al. 2013; Pierens et al. 2013). This could in principle produce a wide gap between planets. However, any phase of late accretion after migration would likely smooth over such a gap. Indeed, in any planetary system it is difficult to account for large gaps between planets (e.g., Raymond et al. 2009).

To conclude this section, we emphasize that local accretion of the Kepler-186 requires the existence of an additional planet between planets e and f. This applies to both in-situ accretion or a late phase of destabilization following inward migration. If there is just one, an additional planet would likely be located at ~ 0.2 AU (the geometric mean between planets e and f).

2.5. Water delivery

Previous work has argued that terrestrial planets orbiting low-mass stars should be relatively dry for two reasons. First, their very short accretion timescales – characterized by high-speed impacts – produce vast amounts of heat that could drive off water (Lissauer 2007; Raymond et al. 2007). Second, given that low-mass stars tend to have lower-mass protoplanetary disks (Andrews & Williams 2007a; Williams & Cieza 2011), the lower-mass bodies that grow in these disks do not provide strong enough gravitational “kicks” to generate the strong radial mixing needed for water delivery (Raymond et al. 2007).

The composition of the Kepler-186 planets cannot be strongly constrained from our accretion simulations because the likely source of water is exterior to the simulation domain. If we assume that a division between inner dry material and outer wet material is located at 2.7 AU for a Sun-like star and that this division scales with the stellar flux, this limit should be located at about 0.5 AU in this system. This division assumes that it is the stellar flux that controls the temperature (and condensation) structure within the disk, although in the inner parts it is more likely to be viscous heating (e.g. Bitsch et al. 2013). Thus, the source of water-rich material may actually be more removed from the habitable zone for low-mass stars than for Sun-like stars, at least assuming a similar disk mass.

Given that the planets are as or more massive than the Solar System’s terrestrial planets, gravitational scattering should make it possible for water-rich material to be scattered from beyond 0.5 AU in to the inner system (Raymond et al. 2007). Indeed, in our simulations the feeding zones of the planets are generally wide and extend to close to the outer edge of our initial conditions. However, the impact speeds remain very high in that region and the accretion timescales short. The only reasonable hope for retaining water is if there were, as discussed above, a phase of inward migration of planetary embryos. In that case the embryos could have formed with large water contents. Their significant masses may have protected them from extensive water loss during giant impacts as well. A measure of the planets’ masses and bulk densities to within a few percent is needed to extract information about the bulk water content.

3. DYNAMICAL STABILITY

A system of two planets in orbit around a star is dynamically stable if their orbits are separated by at least 3.5 mutual Hill radii $R_{H,m}$ (Marchal & Bozis 1982; Gladman 1993). The mutual Hill radius is defined as $R_{H,m} = 1/2 (a_1 + a_2) [(m_1 + m_2)/3M_\star]^{1/3}$, where subscripts 1 and 2 refer to the two planets, a is the orbital semimajor axis, m is the planet mass, and M_\star is the stellar mass. A system of many planets must be more widely separated than a critical limit of 5-10 mutual Hill radii to ensure long-term stability (Chambers et al. 1996; Marzari et al. 2002).

The masses of the Kepler-186 planets are of course unknown. Table 3 lists the planets’ masses for the widest plausible range in compositions, calculated with the mass-radius relations of Fortney et al. (2007). We assumed that the planets are solid and do not contain enough H/He gas to alter their radii (Weiss et al. 2013a; Weiss & Marcy 2014).

The dynamical inter-planet spacing depends on the planets’ true masses. Planets d and e are dynamically closest together and planets e and f are the most widely spaced. Lower-density, lower-mass planets are more widely spaced in dynamical terms (mutual Hill radii). For pure ice, planets d and e are separated by $15R_{H,m}$, but this value decreases with increasing planet mass to $9R_{H,m}$ for Earth-like compositions and just $6.5R_{H,m}$ for pure iron planets. The gap between planets e and f is wide enough to fit another planet. For ice-rock-Earth-iron planets, the gap is 55-37-34-25 mutual Hill radii wide. It is therefore not surprising that our accretion simulations formed extra planets in this region.

The Kepler-186 system is dynamically stable. We ran a suite of N-body simulations of the five-planet system for the full range of planetary compositions. Given the weak constraints on the planets’ eccentricities and longitudes of pericenter, we sampled a range of orbital phases and included initial eccentricities up to 0.05. In all cases the systems were stable for the 0.1 Myr duration. We ran 10 longer-term simulations (without tides or general relativity) with pure iron planets, all of which were stable for 100 Myr.

4. TIDAL ORBITAL EVOLUTION

Given the proximity of the system to its star, tidal interactions are important in shaping the long-term dynamical evolution of the system. Tides affect a close-in planet’s orbit in several ways. On short timescales they drive the system to an equilibrium rotation state, typically either a spin-orbit resonance or a “pseudo-synchronous” state whereby the planet co-rotates with the star at its closest approach (Hut 1981; Ferraz-Mello et al. 2008; Makarov & Efroimsky 2013). Dissipation within the planet decreases the planet’s eccentricity and obliquity. Changes in orbital distance, driven by dissipation in the planet or star, occur on longer timescales.

In multiple-planet systems with close-in planets the orbital evolution is a combination of eccentricity pumping from planet-planet gravitational forcing and damping from tidal interactions (Mardling 2007; Bolmont et al. 2013). The strength of eccentricity pumping is determined by the planets’ masses and orbits and the degree of tidal dissipation by the (unconstrained) dissipation rates,

especially the planet with the strongest dissipation (usually but not always the closest-in one).

We simulated the long-term dynamical and spin evolution of the Kepler-186 system. Our simulations included the tidal dissipation model of Hut (1981) and Leconte et al. (2010) a post-Newtonian precession term (Kidder 1995). Both were applied to all five planets. The code is a fully 3-D version of the one used in Bolmont et al. (2013) to which we also added the effect of the rotation-induced flattening of the star and of the planets (such as in Murray & Dermott 1999; Correia & Rodríguez 2013).

4.1. Exploring the planets' mass range

In order to have a vision as broad as possible on the dynamical evolution of the Kepler-186 system, and as the masses of the planets are not constrained, we performed simulations assuming various compositions for planets.

We first tested the extremes: 100% ice planet and 100% iron planets. Both cases are very unlikely if not impossible but they allow us to investigate the evolution of the system for very low mass planets and very high mass planets. We also tested some intermediate compositions: 50% ice- 50% rock and Earth-like composition. The corresponding masses are stated in Table 3.

We assumed that the 100% ice planets have a dissipation $k_2\Delta t$ higher than that of the Earth¹ (e.g., McCarthy & Castillo-Rogez 2013). We also assume that the 100% iron planets have a dissipation $k_2\Delta t$ higher than that of the Earth (e.g., Koot & Dumberry 2011; Jackson et al. 2000). For these two compositions, we tested 1 and $10\times k_{2,\oplus}\Delta t_{\oplus}$. For intermediate compositions, we tested 0.1 and $1\times k_{2,\oplus}\Delta t_{\oplus}$. The planets were given randomly-chosen orbital angles, initial eccentricities less than 0.06, initial inclinations less than 0.4° ² and obliquities less than 30° .

Figure 8 shows the evolution of the planetary spins during a 10 Myr simulation, assuming Earth-like compositions for all the planets and $k_2\Delta t$ values equal to Earth's. The timescale for tidal interactions is short enough for the four inner planets' evolution to be significantly affected by tides on Myr timescales. The obliquities of the four inner planets were reduced to nearly zero within ~ 1 Myr, regardless of composition and tidal dissipation. Likewise, the rotation rates of the four inner planets converged to their pseudo-synchronous values (dashed lines). Given their small eccentricities, this means that the planets rotate extremely slowly, effectively synchronously. Kepler-186f is evolving towards pseudo-synchronization, and due to the short initial rotation period its obliquity starts increasing. On the long term, the rotation period of Kepler-186f lengthens and its obliquity starts to decrease toward its (near zero) equilibrium value.

Figure 9 shows the system's tidal evolution timescales for set \mathcal{A} . The timescales are shown for each planet and for the different compositions assuming the lower values of $k_2\Delta t$: 1, 0.1, $0.1\times k_{2,\oplus}\Delta t_{\oplus}$ for 100% ice, 50%-50% rock ice, Earth composition and 100% iron planets respectively. A combination of lower masses and a

¹ k_2 is the Love number of degree 2 and Δt is the time lag (see Hut 1981). $k_2\Delta t$ is assumed constant. For Earth, $k_{2,\oplus}\Delta t_{\oplus} = 213$ s (Neron de Surgy & Laskar 1997).

² We choose small initial inclinations so as to ensure that Kepler-186f transits.

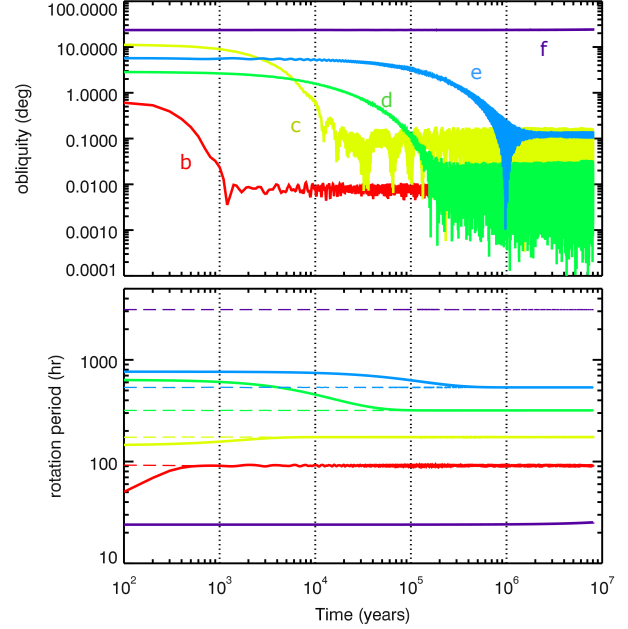


FIG. 8.— Evolution of the five planets' obliquities (top) and rotation periods (bottom) for set \mathcal{A} . In the bottom plot, the solid lines correspond to the planets' actual spin periods and the dashed lines to the pseudo-synchronous values. Given their small orbital eccentricities, the pseudo-synchronous rotation states are very close to 1:1 spin-orbit synchronous rotation. The timescale for tides is strongly dependent on the orbital radius. The ordering of the planets is clearly discernible from the order in which their obliquities decay.

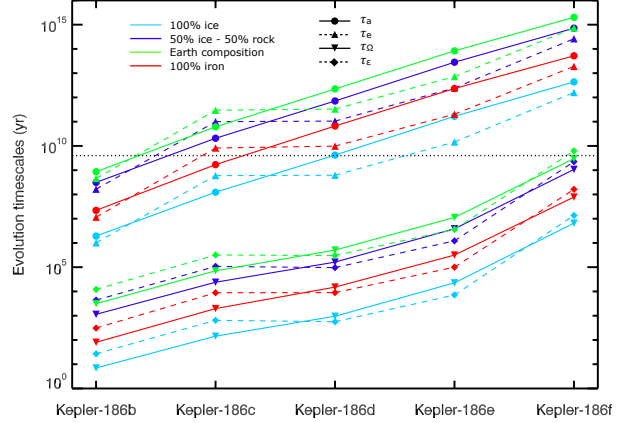


FIG. 9.— Timescales for planetary-tide induced evolution for the Kepler-186 system and for the four compositions considered here. τ_a , τ_e , τ_Ω and τ_ϵ are respectively the timescales of evolution of semi-major axis, eccentricity, rotation rate and obliquity. The horizontal black dotted line corresponds to the estimated system age of 4 Gyr. The timescales were computed here for set \mathcal{A} , however the timescales of evolution for set \mathcal{B} are of the same order of magnitude.

rather high dissipation rates makes the tidal evolution timescales much shorter for pure ice planets than for the other compositions. The evolution timescales computed for set \mathcal{B} are of the same order of magnitude and those computed with set \mathcal{B} .

Constraining the age of the system would allow us to possibly constrain the compositions of the planets. Indeed, the timescale for the semi-major axis evolution of Kepler-186b is quite short – assuming a composition of 100% ice and 100% iron – meaning that such a planet

would be falling on its host star in timescales that are probably shorter than the system lifetime. It is therefore more probable that the composition of Kepler-186b– and also of Kepler-186c– is rocky.

The evolution timescales of the semi-major axis and eccentricity of Kepler-186e and Kepler-186f are higher than the age of the Universe. For rocky compositions, the evolution timescales of the semi-major axis and eccentricity of Kepler-186c and Kepler-186d are also longer than the age of the Universe. We then expect the four outer planets to have been formed about where they are now located. However, Kepler-186b is likely to have been formed a bit further away

4.2. An extra planet?

An extra planet could exist in the Kepler-186 system between Kepler-186e and Kepler-186f (see section 3.3). We therefore simulated the dynamical evolution of the system adding an inclined extra planet in order to see its influence on the observable planets. We performed these simulations assuming Earth-like compositions and a $k_2\Delta t = 0.1 \times k_{2,\oplus}\Delta t_\oplus$ for planets b, c, d, e and f.

We considered an extra planets with mass between $0.1M_\oplus$ and $1M_{Jup}$. The rocky planets (from 0.1 to $10 M_\oplus$) have a $k_2\Delta t$ of $0.1 \times k_{2,\oplus}\Delta t_\oplus$. The Neptune mass planet has a $k_2\Delta t$ of 0.038 s and the Jupiter mass planet has a $k_2\Delta t$ of 7×10^{-5} s. The extra planet has a semi-major axis of 0.233 AU, an initial eccentricity of 0.01 and an initial inclination of 2° so as not to transit. Its initial obliquity is of 17° and its initial rotation period is of 24 hr.

The accretion simulations in Section 2 tells us that the mass range should probably be narrower but we chose here not to constrain the parameter space.

Table 4 shows a measure of the observability of the planets in the simulations: the transit probability is the fraction of the simulation during which each planet has an inclination lower than $\arctan(R_\star/a)$, where a is the planets' semi-major axis. The values of the inclination above which the transit is geometrically impossible is for each planet (b, c, d, e, extra planet and f): $3.5, 2.3, 1.5, 1.1, 0.60, 0.34^\circ$ for set \mathcal{A} and $3.3, 2.2, 1.5, 1.0, 0.58, 0.32^\circ$ for set \mathcal{B} .

Due to the initial small eccentricity of the extra planet, the eccentricities of planets b, c, d, e and f are not excited to levels incompatible with the observations. In particular, the eccentricity of Kepler-186f remains always below 0.03. However, the inclination is excited by the presence of the extra planet and the more massive the extra planet the higher the other planets' inclinations.

Adding a massive non-transiting planet decreases the probability of transit of Kepler-186f considerably: it decreases from 88% when the extra planet is $0.1 M_\oplus$ to 33% when the planet is $1 M_\oplus$. It is therefore unlikely that the system hosts a planet more massive than $1 M_\oplus$ between Kepler-186e and Kepler-186f. Figure 10 shows the evolution of the system with an extra $1 M_\oplus$ planet after 6 Myr of integration. The bottom plot shows the limit inclination over which Kepler-186f does not transit (dashed purple line). The inclination of Kepler-186f oscillates and sometimes becomes greater than the limit $\arctan(R_\star/a_f)$.

Adding a planet in the system allows angular momentum to transfer to the outer planet much more efficiently

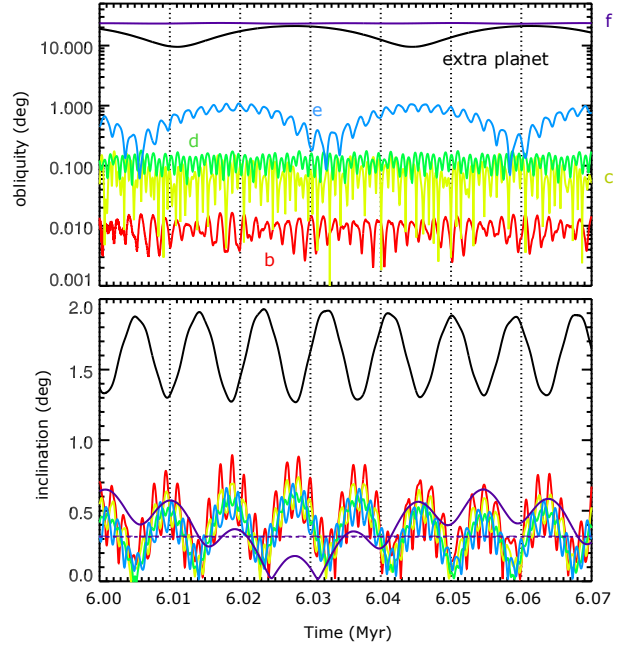


FIG. 10.— Snapshot of the evolution of the obliquities and inclinations of the six planets over 70,000 yrs (set \mathcal{B}). The colored lines correspond to the five confirmed planets (from red to purple: from b to f), and the black line corresponds to the hypothetical extra planet ($1 M_\oplus$). In the bottom plot the purple dashed line corresponds to the limit inclination over which Kepler-186f does not transit.

and this has an influence on its obliquity. Figure 10 shows the evolution of the system with an extra $1 M_\oplus$ planet. We can see that instead of having a purely tidal evolution, the obliquity of Kepler-186f oscillates between 23° and 24° with a main frequency of $\sim 10^4$ yr. If the extra planet is $10 M_\oplus$, the obliquity of Kepler-186f oscillates 18° and 24° . Oscillations of the planet's obliquity would have an influence on the planet's climate (e.g., Armstrong et al. 2014).

An extra $1 M_\oplus$ planet also affects the equilibrium obliquities of the four inner planets. The influence is greater for Kepler-186e and Kepler-186d, but they all stay below 1° .

When the mass of the extra planet is larger, the obliquities of the planets are higher and can reach values of a few degrees. Tides are less efficient to counteract the excitation due to the high mass extra planet.

4.3. Evolution of Kepler-186f

With no extra planet in the system, Kepler-186f is dynamically isolated from the four inner planets. Its orbit and spin evolve due to the tides it raises on the star and those raised in it by the star rather than gravitational interactions with other planets.

Figure 11 shows the evolution of the eccentricities and obliquities of the five planets over the last 5,000 years of the simulation from Fig. 8. The eccentricity and obliquity of Kepler-186f do not undergo noticeable oscillations whereas the four inner planets' do. Their eccentricities oscillate as a combination of frequencies that correspond to the secular modes of the system (see, for example, Murray & Dermott 1999). The amplitudes of oscillation are a few percent and the characteristic secular timescales are $\sim 1,000$ years. The oscillation amplitudes

TABLE 4
PROBABILITY OF TRANSIT FOR SET \mathcal{B} .

Mass of extra planet	Prob. of transit (calculated for a 10 Myr simulation)					
	Kepler-186b	Kepler-186c	Kepler-186d	Kepler-186e	extra planet	Kepler-186f
0.1 M_{\oplus}	100%	100%	100%	100%	0%	88%
1 M_{\oplus}	100%	100%	100%	100%	0%	33%
10 M_{\oplus}	95%	68%	46%	30%	13%	4%
1 M_{Neptune}	74%	49%	38%	19%	0%	3%
1 M_{Jupiter}	52%	42%	27%	17%	0%	5%

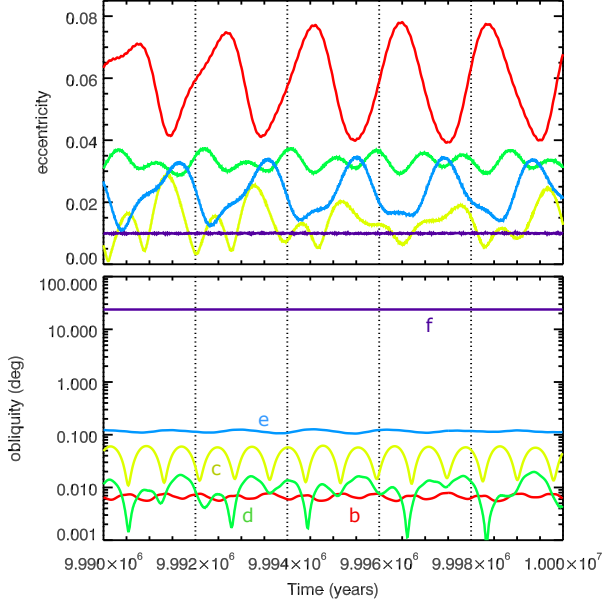


FIG. 11.— Short-term (10,000 year) evolution of the eccentricities (top) and obliquities (bottom) of the five planets in the Kepler-186 system (set \mathcal{B}).

are mass-independent but the frequencies increase linearly with the planet masses. Oscillations in eccentricity can cause a modest change in the insolation received by a planet, as the orbit-averaged insolation scales with eccentricity e as $(1 - e^2)^{-1/2}$. This in turn can in some instances trigger changes in the planetary climate on the secular timescale (Spiegel et al. 2010). Indeed, large climatic events are thought to correlate with oscillations of Earth’s orbital quantities, especially its eccentricity and obliquity (so-called “Milankovitch cycles”; Berger 1988).

Figure 9 shows that the planetary tide does not cause the eccentricity and semi-major axis of Kepler-186f to evolve on timescales shorter than 10 Gyr³. However, the evolution timescales for the obliquity and rotation period are of the order of magnitude of 1 Gyr for rocky compositions. So given the age of the system, Kepler-186f could have reached pseudo-synchronization and very low obliquity or could be still evolving.

Fig. 8 shows the very slow tidal evolution of Kepler-186f. Over 10 Myr Kepler-186f retains its initial obliquity, rotation rate and eccentricity. However, toward the end of the simulation Kepler-186f’s rotation appears to be slowly decreasing and its obliquity slowly increasing.

We calculated several possible long-term evolutionary pathways for Kepler-186f’s spin state. The initial obliq-

³ The stellar-tide induced evolution occurs on timescales even longer: $> 10^{17}$ yr.

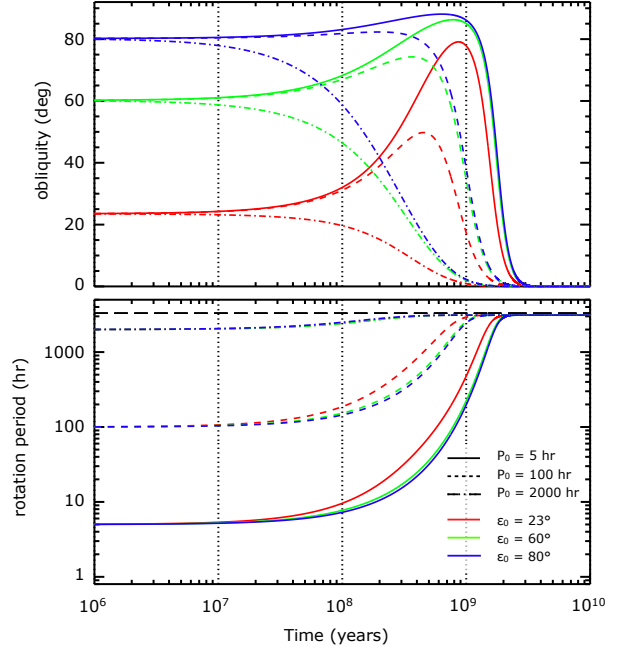


FIG. 12.— Long-term evolution of the obliquity (top) and rotation period (bottom) of Kepler-186f (set \mathcal{A}). Each set of linestyle curves represents a different initial spin rate, each set of colored curves represents a different initial obliquity. The thick black dashed line represents the pseudo-synchronous rotation which, for this zero-eccentricity example, is the 1:1 spin-orbit resonance. The fastest-spinning (red full line) curve is closest to the example shown in Fig. 8.

uity was varied from Earth’s current obliquity of 23.5° to an obliquity of 80° and the initial spin rate was varied over a span of two orders of magnitude. The planet is here assumed to have the same dissipation factor $k_2 \Delta t$ as Earth. Unlike the simulations from Figs 8 and 11, these calculations were performed with only Kepler-186e and Kepler-186f in the system. They were nonetheless a fully-3D implementation of the *constant time lag* equilibrium tidal model (Hut 1981; Leconte et al. 2010).

Figure 12 shows that planet f’s obliquity increases for all but the slowest initial spin rate. The period of obliquity increase lasts for a few hundred Myr. It is followed by a long slow decay that lasts 2-3 Gyr (for the arbitrarily chosen range of initial spin rates), broadly consistent with the results of Heller et al. (2011). The initial obliquity and spin rates are of course unknown, although N-body simulations of terrestrial accretion produce planets with fast initial spins and an isotropically-distributed obliquities (Kokubo & Ida 2007).

Evolution timescales scale inversely with the planet’s dissipation rate, assumed here to be roughly Earth-like. Stronger dissipation accelerates the evolution whereas

weaker dissipation slows it down. The age of Kepler-186 is thought to be higher than a few Gyr, so assuming an Earth dissipation, it would mean that Kepler-186f should be in a pseudo-synchronous rotation state with a small obliquity. However, the age of the system is unconstrained. So if Kepler-186 is somewhat younger (say 1 Gyr) or if the dissipation within planet f is inefficient⁴, then Kepler-186f should not have reached a pseudo-synchronous state. In that case, although Kepler-186f's spin rate would probably have slowed to within a factor of a few of the pseudo-synchronous rate, its obliquity would be unconstrained and could assume very high values ($\sim 85^\circ$ for the full blue line of Figure 12).

5. HABITABILITY OF KEPLER-186F

Given the enormous distances to potentially life-bearing exoplanets, extraterrestrial life will only be detectable – at least in the near-term future – if it has become a global phenomenon and influenced both the atmosphere and the surface of the planet at large scales (both in time and in space). If this is the case, the detection of biosignatures might be possible (e. g., Sagan et al. 1993; Des Marais et al. 2002). The energy required to change atmospheric composition and sustain (detectable) chemical disequilibria is most likely only provided by photosynthesis which uses starlight as an energy source (on Earth, the amount of solar radiation is more than four orders of magnitude larger than geothermal energy). Aphotic habitats, such as are hypothesized for the possible subsurface ocean of Europa (e.g., Hussmann et al. 2006), will be difficult or even impossible to detect.

The classical habitable zone (HZ, e.g., Dole 1964; Hart 1978; Kasting et al. 1993; Selsis et al. 2007; Kopparapu et al. 2013) focuses on surface life. Acknowledging the fact that all terrestrial life needs liquid water, the HZ is defined as the region around a star where a terrestrial planet can host liquid water on the surface. The extent of this HZ naturally depends on the atmospheric conditions (composition, pressure) as well as on the properties of the central star.

Many factors influence the width of the HZ, such as the geological activity (e.g., Lammer et al. 2010), the biosphere itself (e.g., Grenfell et al. 2010) or the dynamical environment of the planetary system (e.g., Jones et al. 2006; Sándor et al. 2007; Kopparapu & Barnes 2010). Other factors include, for example, the central star, planetary mass and radius, atmospheric composition or atmospheric pressure (e.g., Selsis et al. 2007; Kopparapu et al. 2013).

Applying approximate equations from Kopparapu et al. (2013) for the Kepler-186 system results in an extent of the HZ from 0.21 AU–0.38 AU. A more optimistic empirical estimate of the width of the habitable zone (Selsis et al. 2007) yields a range from 0.15 AU–0.42 AU. This suggests that within the uncertainties of its orbital distance Kepler-186f is indeed in the HZ.

In terms of insolation, Kepler-186f receives $S_{K186} = 0.32^{+0.05}_{-0.03}$ times the insolation as present

Earth. Within 1- σ uncertainty, this is the same insolation ($S_{G581} = 0.29$) as that received by the super-Earth candidate GJ 581d, which climate models have shown to be capable of having liquid water on its surface (e.g., Wordsworth et al. 2010; von Paris et al. 2010; Hu & Ding 2011; Kaltenegger et al. 2011; Wordsworth et al. 2011), given a large enough CO₂ greenhouse effect ($p_{CO_2} \gtrsim 1\text{--}2$ bar).

For a preliminary assessment of the habitability of Kepler-186f, we used the one-dimensional, cloud-free radiative-convective atmosphere model from von Paris et al. (2010). Model atmospheres were assumed to be composed of CO₂, N₂ and H₂O only. We performed a series of calculations, varying planetary gravity, insolation as well as N₂ and CO₂ partial pressures. Input parameters are listed in Table 5. The assumed range of CO₂ and N₂ partial pressures is plausible if Kepler-186f is a rocky planet. The volatile budget of Earth is thought to consist of several bars of N₂ and tens to hundreds of bar of CO₂ (e.g., Turekian & Clark 1975; Kasting 1988; McKay & Stoker 1989; Lundin & Barabash 2004; Goldblatt et al. 2009). The needed stellar input spectrum for the model simulations was calculated from a synthetic spectrum using stellar models from Hauschildt et al. (1999), stellar parameters from Table 1 and a metallicity of -0.28 (Quintana et al. 2014).

Figure 13 shows the calculated surface temperatures as a function of CO₂ partial pressure for different N₂ partial pressures. These results clearly suggest that Kepler-186f is a potentially habitable planet. To reach mean surface temperatures above freezing, modest amounts of CO₂ are needed for most of the cases. For a large atmospheric reservoir of N₂, surface temperatures rise above 273 K already at about 200–500 mbar of CO₂, again for almost every scenario.

Our results do not show a maximum greenhouse effect for CO₂ (Kasting et al. 1993), i.e. surface temperatures continue to rise with increasing CO₂ (although the slope of the lines in Fig. 13 decreases with increasing CO₂). This is consistent with other atmospheric models of planets orbiting M stars (e.g., Wordsworth et al. 2010; von Paris et al. 2010). The reason for this behavior is the presence of large amounts of water in the atmosphere which decreases the albedo (due to absorption of near-IR radiation) and increases the surface temperature (due to a strong greenhouse effect). Additionally, the contribution of Rayleigh scattering to the total energy budget is somewhat negligible given that Kepler-186 is a much cooler star than the Sun and consequently emits less radiation in the UV-visible part of the spectrum. Hence, cooling associated with a higher albedo due to Rayleigh scattering is less efficient.

Furthermore, results shown in Fig. 13 imply a strong influence of N₂ on calculated surface temperatures, consistent with results in previous studies (e.g., Li et al. 2009; Goldblatt et al. 2009; von Paris et al. 2010; Wordsworth et al. 2010; von Paris et al. 2013). High N₂ partial pressures could reduce the amount of CO₂ needed to maintain a surface temperature above freezing by almost an order of magnitude.

As can be inferred from Fig. 13, a change in gravity due to uncertainties in stellar radius, transit depth and planetary mass (Tables 1–3) has a modest influence on calculated surface temperatures. With increasing

⁴ It is likely that the dissipation of Kepler-186f is actually lower than that of the Earth, so the curves of Figure 12 could be shifted to the right, meaning that the state of pseudo-synchronization and low obliquity occurs later.

gravity, surface temperatures decrease by 5-10 K. This is mainly due to a decrease in column density (at fixed pressure), consistent with previous studies (e.g., Wordsworth et al. 2010; Rauer et al. 2011). Generally, assuming that Kepler-186 f is indeed a rocky planet, mass and radius estimates, hence planetary gravity, are not found to be critical for habitability.

From Table 1 (or, e.g., Table 1 in Borucki et al. (2011)), it is apparent that the stellar mass and radius are not constrained at very high precision (partly due to the faintness of Kepler-186). Since stellar mass directly impacts planetary orbital distance (via Keplers Third Law) and stellar radius is related to the luminosity, insolation for Kepler-186 f varies by as much as 20% for Sets *A*, *B* or orbital distances as stated in Quintana et al. (2014). Naturally, this has a certain impact on calculated surface temperatures, as shown in Fig. 13. Upon increasing stellar insolation, surface temperatures increase by 10-60 K, depending on CO₂ and N₂ partial pressure. This is a much larger effect than for gravity. Taking for example Set *B* at high gravity (lower right in Fig. 13), a minimum of 1 bar N₂ is required to reach habitable surface temperatures even when assuming 10 bar of CO₂. Hence, our results emphasize the need of accurately determined stellar parameters for habitability studies.

Calculated surface temperatures in Fig. 13 rise up to 350-370 K for high-pressure atmospheres. Such high temperatures are not conducive for higher lifeforms on Earth, although extremophiles are known that can thrive under these conditions (Rothschild & Mancinelli 2001). Another potential challenge for lifeforms might be the increased pH value of rain due to high amounts of atmospheric CO₂ (e.g., Ohmoto et al. 2004) which again is in principle tolerated by some extremophile species on Earth (Rothschild & Mancinelli 2001). Therefore, it is at least conceivable from an Earth-centric view that a microbial biosphere could exist under the atmospheric and surface conditions calculated for Kepler-186 f.

A further interesting field of investigation would be the possibility of photosynthesis occurring on Kepler-186 f. A number of previous studies has studied the potential for (an)oxygenic photosynthesis on planets orbiting M stars (e.g., Heath et al. 1999; Kiang et al. 2007). They found that photosynthesis is indeed possible, however yielding less net productivity. Figure 14 shows the net surface radiative flux as a function of wavelength for a specific model scenario ($p_{CO_2}=5$ bar, $p_{N_2}=1$ bar, $g=11.8$ ms⁻²) of Set *B*. The surface temperature for this specific case is 285 K, close the modern Earth. For comparison, also values for modern Earth are shown. Also indicated are positions of photosynthetic pigments used by terrestrial biota. It is clearly seen that Earth's surface receives much more radiative energy than the surface of Kepler-186 f (about a factor of 7 for the integrated flux). At wavelengths around 500-700 nm (corresponding to plant chlorophyll), the difference is even more pronounced with modern Earth receiving 10-20 times more flux than Kepler-186 f. This suggests that even if Kepler-186 f is indeed habitable and life emerged, it is likely less productive than on Earth, in accordance with previous work. This implies that detection of biosignatures is probably more difficult than for Earth-analogs. However, note that photosynthesis on Earth uses only a small

fraction of the actually available sunlight (a few to a few tens of percent, e.g., Heath et al. 1999).

The four inner planets do not lie in the habitable zone. Their orbits remain interior to the inner boundary of the optimistic model. However, it remains possible that Kepler-186e could have liquid water on its surface. If Kepler-186e has significant cloud cover, its albedo is increased and the inner edge of the habitable zone can be pushed far inward of the optimistic criterion, in to ~ 0.5 AU for a Sun-like star (Selsis et al. 2007). The fact that Kepler-186e's rotation is virtually synchronized with its orbit may also increase the planets chance of being habitable. Yang et al. (2013) showed that clouds in the atmospheres of tidally-locked planets tend to cluster at the sub-solar point and create a net cooling effect.

An orbit within the habitable zone does not make a planet habitable. Venus' and Mars' orbits are both within certain estimates of the habitable zone but neither is thought to harbor life. In addition, the extent of the habitable zone itself is uncertain. It has been claimed that there is no real outer boundary to the habitable zone. The strong greenhouse effect of H₂-dominated atmospheres dominated can possibly extend the habitable zone to an almost indefinite orbital distance (e.g., Stevenson 1999; Pierrehumbert & Gaidos 2011; Wordsworth 2012).

Many other factors are required for a planet to be considered capable of hosting life (e.g., available nutrients, magnetic fields, see e.g. Schulze-Makuch et al. 2011). Even the list of factors for habitability is poorly constrained. For example, the planet must have an adequate reservoir of volatiles, including water. Given their rapid energetic accretion, water retention may in fact be a concern for planets orbiting low-mass stars (e.g., Lissauer 2007; Raymond et al. 2007). It has also been proposed that plate tectonics is a key factor for maintaining a stable climate via the carbonate-silicate cycle (Walker et al. 1981). This may require a minimum internal heat flux from either radioactive decay of long-lived isotopes (Williams et al. 1997a) or tidal heating (Barnes et al. 2009).

As has been shown in Sect. 4 (see also, e.g. Fig. 12), the rotation period of planet f is likely of the order of days to weeks, even a complete 1:1 synchronization with the orbital period seems possible. If such synchronization did indeed happen, the planet possess permanent day- and nightsides. However, many previous studies show that slowly rotating planets likely have small latitudinal and longitudinal temperature gradients given atmospheric pressures of at least a few tens of millibars (e.g., Joshi et al. 1997; Joshi 2003; Spiegel et al. 2008; Wordsworth et al. 2011)). Therefore, at least in terms of surface temperature and atmospheric collapse, the habitability of planet f is not hindered by its increasing rotation period. Another possible concern is the potentially very high obliquity for extended periods of time (Fig. 12). However, modeling studies by, e.g., Williams et al. (1997b) or Spiegel et al. (2009), suggest that high-obliquity climates are not necessarily an impediment to habitability. Furthermore, because of the very efficient energy transport to be expected for slow rotators, uneven stellar irradiation caused by high obliquity values will not influence habitability much.

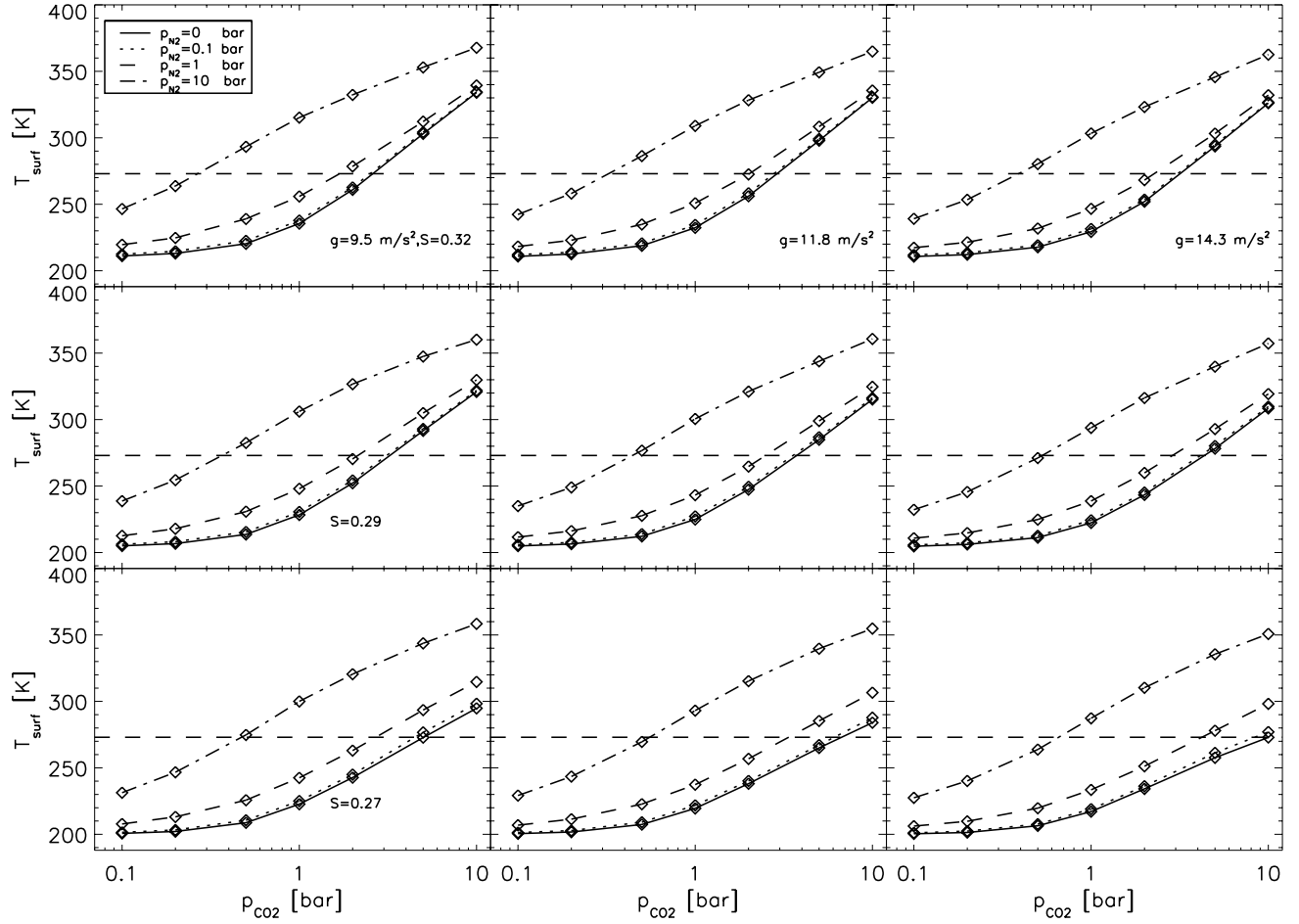


FIG. 13.— Surface temperature as a function of CO₂ partial pressure, for different N₂ partial pressures. Water triple point temperature of 273 K indicated by horizontal dashed line. Top to bottom rows: decreasing insolation (from top to bottom: Quintana et al. 2014, Set A, Set B from Table 1). Left to right columns: increasing gravity.

TABLE 5
ATMOSPHERIC MODEL INPUT PARAMETERS.

Parameter	Value	Comment
Insolation	0.27-0.32 S_{\oplus}	Quintana et al. (2014) and Table 1
Gravity	9.5-14.3 ms^{-2}	range calculated from Table 2 and Table 3
p_{CO_2}	0.1-10 bar	low estimates for Earth inventory
p_{N_2}	0-10 bar	uncertainty range for Earth
Surface albedo	0.13	modern Earth value, Rossow & Schiffer (1999)
Relative humidity	Manabe & Wetherald (1967)	used by von Paris et al. (2010) and Wordsworth et al. (2010)

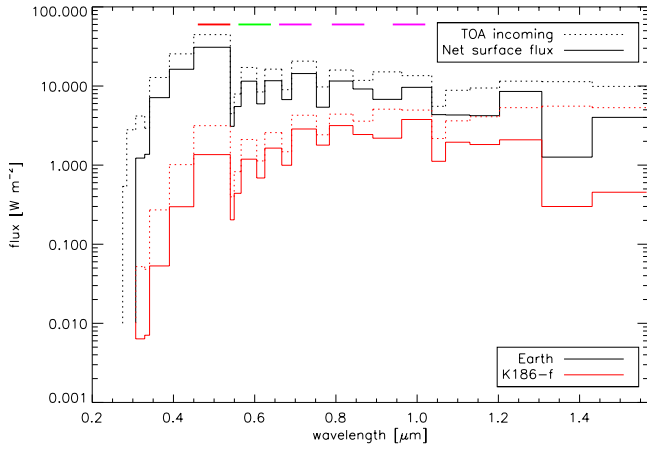


FIG. 14.— Net stellar flux at the surface for Set \mathcal{B} ($p_{\text{CO}_2}=5$ bar, $p_{\text{N}_2}=1$ bar, $g=11.8 \text{ ms}^{-2}$), compared to modern Earth. Color bars indicate positions of photosynthetic pigments used by terrestrial biota.

6. DISCUSSION/CONCLUSIONS

We have presented an extensive study of the formation, orbital dynamics, tidal evolution, and habitability of the Kepler-186 system.

In section 2 we presented a simple end-to-end analysis of the accretion of the system. Using the planets' orbital configuration we built two minimum-mass disks. We then attempted to reproduce the system's orbital architecture. We performed simulations of in-situ accretion from these disks, which we interpret as having been shaped by a previous episode of orbital migration. The mass-orbital radius distribution of our simulations provided a modestly-good match to the real system, although neither set of simulations adequately match both the four inner planets and the outer one. The planets also tended to have inclinations that were too large to be consistent with five planets in transit.

Perhaps most striking is that our accretion simulations systematically formed too many planets. At least one, and often two, planets tend to form between the orbits of Kepler-186e and Kepler-186f. From our dynamical simulations (Section 4.2), we can infer that if such a planet exists, it should be less massive than $1 M_{\oplus}$ otherwise its gravitational influence on Kepler-186f would most likely prevent Kepler-186f from transiting.

Given that the system is probably older than a few Gyr, simulations of tidal evolution show that the four inner planets of the system are in pseudo-synchronous rotation (respectively, $P_{\text{rot}} = \sim 4, \sim 7, \sim 13, \sim 22$ and ~ 130 days) with very low obliquities ($< 1^\circ$). However, in a few simulations the obliquity of Kepler-186d was excited to more than 10° due to a brief but deep crossing of the 5:3 mean motion resonance between Kepler-186c

and Kepler-186d. The competition between the excitation due to planet-planet gravitational interactions and tidal damping has the effect of stabilizing this relatively high obliquity on ~ 10 Myr timescales.

We also showed that given the uncertainties on the age of the star as well as the uncertainties on the composition and tidal dissipation, the rotation state of Kepler-186f is unconstrained. If the system is somewhat younger – 1 Gyr old – or if the tidal dissipation of Kepler-186f is lower than that of Earth's, Kepler-186f could still be in the process of pseudo-synchronization and its obliquity could be high. However, if the system is about 4 Gyr old or the tidal dissipation of Kepler-186f is Earth-like, Kepler-186f would be pseudo-synchronized with a long rotation period (~ 130 days). The variety of spin states of Kepler-186f should then be investigated by exoplanet-climate modelers.

The dynamics of the system would be affected if, as predicted by the accretion simulations, an additional planet existed between Kepler-186e and Kepler-186f. Without this additional planet, Kepler-186f is relatively isolated from the inner system, so its eccentricity and obliquity oscillations have a very low amplitude. However, an extra planet allows angular momentum to transfer from the inner parts of the system to Kepler-186f, causing higher amplitude oscillations of eccentricity and obliquity.

Regarding the thermal history of Kepler-186f, simulations show that the tidal heat flux could be sustained at values of more than 0.1 W/m^2 for at least the first 10 Myr of evolution (assuming Earth composition, $k_{2,\oplus} \Delta t_{\oplus}$) and more than 1 W/m^2 for the first 10^5 yr of evolution (assuming pure ice composition, $10 \times k_{2,\oplus} \Delta t_{\oplus}$). However, atmospheric modeling results from Sect. 5 suggest that even for dense atmospheres, the radiative flux at the surface exceeds the tidally induced fluxes by at least a factor of ten.

In Sect. 5 we presented atmospheric model calculations which indicate that Kepler-186f is indeed squarely situated in the HZ around Kepler-186, with relatively modest amounts of CO_2 and N_2 .

The authors would like to thank Gabriel Tobie for useful discussion on planets dissipation.

S.N.R. and F.H. are grateful to the Agence Nationale pour la Recherche via grant ANR-13-BS05-0003-02 (project MOJO). S.N.R.'s contribution was performed as part of the NASA Astrobiology Institute's Virtual Planetary Laboratory Lead Team, supported by the NASA under Cooperative Agreement No. NNA13AA93A.

This research has been partly supported by the Helmholtz Association through the research alliance "Planetary Evolution and Life". This study has received financial support from the French State in the frame of the "Investments for the future" Programme IdEx Bordeaux, reference ANR-10-IDEX-03-02.

REFERENCES

- Andrews, S. M., & Williams, J. P. 2007a, *Astrophys. J.*, 671, 1800
- , 2007b, *Astrophys. J.*, 659, 705
- Armstrong, J. C., Barnes, R., Domagal-Goldman, S., & Planetary Laboratory, V. 2014, in *American Astronomical Society Meeting Abstracts*, Vol. 223, American Astronomical Society Meeting Abstracts, 325.08
- Barnes, R., Jackson, B., Greenberg, R., & Raymond, S. N. 2009, *Astrophys. J. Letters*, 700, L30
- Batalha, N. M., Borucki, W. J., Bryson, S. T., et al. 2011, *Astrophys. J.*, 729, 27
- Berger, A. 1988, *Reviews of Geophysics*, 26, 624

- Bitsch, B., Crida, A., Morbidelli, A., Kley, W., & Dobbs-Dixon, I. 2013, *Astron. Astrophys.*, 549, A124
- Boley, A. C., & Ford, E. B. 2013, arXiv:1306.0566, arXiv:1306.0566
- Bolmont, E., Selsis, F., Raymond, S. N., et al. 2013, *Astron. Astrophys.*, 556, A17
- Borucki, W. J., Koch, D., Basri, G., et al. 2010, *Science*, 327, 977
- Borucki, W. J., Koch, D. G., Basri, G., et al. 2011, *Astrophys. J.*, 736, 19
- Borucki, W. J., Koch, D. G., Batalha, N., et al. 2012, *Astrophys. J.*, 745, 120
- Borucki, W. J., Agol, E., Fressin, F., et al. 2013, *Science*, 340, 587
- Chambers, J. E. 1999, *Monthly Not. Royal Astron. Soc.*, 304, 793
- Chambers, J. E., Wetherill, G. W., & Boss, A. P. 1996, *Icarus*, 119, 261
- Chatterjee, S., & Tan, J. C. 2014, *Astrophys. J.*, 780, 53
- Chiang, E., & Laughlin, G. 2013, *Monthly Not. Royal Astron. Soc.*, 431, 3444
- Correia, A. C. M., & Rodríguez, A. 2013, *Astrophys. J.*, 767, 128
- Cossou, C., Raymond, S., & Pierens, A. 2013, ArXiv e-prints, arXiv:1302.2627
- Cossou, C., Raymond, S. N., & Pierens, A. 2014, in *IAU Symposium*, Vol. 299, IAU Symposium, ed. M. Booth, B. C. Matthews, & J. R. Graham, 360–364
- Des Marais, D. J., Harwit, M. O., Jucks, K. W., et al. 2002, *Astrobiology*, 2, 153
- Dole, S. H. 1964, *Habitable planets for man* (New York, Blaisdell Pub. Co. [1964] [1st ed..])
- Fang, J., & Margot, J.-L. 2012, *Astrophys. J.*, 761, 92
- Ferraz-Mello, S., Rodríguez, A., & Hussmann, H. 2008, *Celestial Mechanics and Dynamical Astronomy*, 101, 171
- Fortney, J. J., Marley, M. S., & Barnes, J. W. 2007, *Astrophys. J.*, 659, 1661
- Fressin, F., Torres, G., Rowe, J. F., et al. 2012, *Nature*, 482, 195
- Gladman, B. 1993, *Icarus*, 106, 247
- Goldblatt, C., Claire, M. W., Lenton, T. M., et al. 2009, *Nature Geoscience*, 2, 891
- Goldreich, P., & Tremaine, S. 1980, *Astrophys. J.*, 241, 425
- Grenfell, J. L., Rauer, H., Selsis, F., et al. 2010, *Astrobiology*, 10, 77
- Haisch, Jr., K. E., Lada, E. A., & Lada, C. J. 2001, *Astrophys. J. Letters*, 553, L153
- Hansen, B. M. S., & Murray, N. 2012, *Astrophys. J.*, 751, 158
- . 2013, *Astrophys. J.*, 775, 53
- Hart, M. H. 1978, *Icarus*, 33, 23
- Hauschildt, P. H., Allard, F., & Baron, E. 1999, *Astrophys. J.*, 512, 377
- Heath, M. J., Doyle, L. R., Joshi, M. M., & Haberle, R. M. 1999, *Origins of Life and Evolution of the Biosphere*, 29, 405
- Heller, R., Lecote, J., & Barnes, R. 2011, *Astron. Astrophys.*, 528, A27
- Hillenbrand, L. A. 2008, *Physica Scripta Volume T*, 130, 014024
- Hu, Y., & Ding, F. 2011, *Astron. Astrophys.*, 526, A135
- Hussmann, H., Sohl, F., & Spohn, T. 2006, *Icarus*, 185, 258
- Hut, P. 1981, *Astron. Astrophys.*, 99, 126
- Jackson, I., Fitz Gerald, J. D., & Kokkonen, H. 2000, *J. Geophys. Res.*, 105, 23605
- Jones, B. W., Sleep, P. N., & Underwood, D. R. 2006, *Astrophys. J.*, 649, 1010
- Jontof-Hutter, D., Lissauer, J. J., Rowe, J. F., & Fabrycky, D. C. 2014, *Astrophys. J.*, 785, 15
- Joshi, M. 2003, *Astrobiology*, 3, 415
- Joshi, M. M., Haberle, R. M., & Reynolds, R. T. 1997, *Icarus*, 129, 450
- Kaltenegger, L., Segura, A., & Mohanty, S. 2011, *Astrophys. J.*, 733, 35
- Kasting, J. F. 1988, *Icarus*, 74, 472
- Kasting, J. F., Whitmire, D. P., & Reynolds, R. T. 1993, *Icarus*, 101, 108
- Kiang, N. Y., Segura, A., Tinetti, G., et al. 2007, *Astrobiology*, 7, 252
- Kidder, L. E. 1995, *Phys. Rev. D*, 52, 821
- Kokubo, E., & Ida, S. 2007, *Astrophys. J.*, 671, 2082
- Kokubo, E., Kominami, J., & Ida, S. 2006, *Astrophys. J.*, 642, 1131
- Koot, L., & Dumberry, M. 2011, *Earth and Planetary Science Letters*, 308, 343
- Kopparapu, R., Ramirez, R., Kasting, J., et al. 2013, *Astrophys. J.*, 765, 131
- Kopparapu, R. K., & Barnes, R. 2010, *Astrophys. J.*, 716, 1336
- Lammer, H., Selsis, F., Chassefière, E., et al. 2010, *Astrobiology*, 10, 45
- Lecote, J., Chabrier, G., Baraffe, I., & Levrard, B. 2010, *Astron. Astrophys.*, 516, A64
- Li, K., Pahlevan, K., Kirschvink, J., & Yung, Y. 2009, *Proceedings of the National Academy of Sciences*, 106, 9576
- Lissauer, J. J. 2007, *Astrophys. J. Letters*, 660, L149
- Lissauer, J. J., Ragozzine, D., Fabrycky, D. C., et al. 2011, *Astrophys. J. Suppl.*, 197, 8
- Lopez, E. D., & Fortney, J. J. 2013, ArXiv e-prints, arXiv:1311.0329
- Lundin, R., & Barabash, S. 2004, *Planet. Space Science*, 52, 1059
- Makarov, V. V., & Efroimsky, M. 2013, *Astrophys. J.*, 764, 27
- Manabe, S., & Wetherald, R. T. 1967, *J. Atmosph. Sciences*, 24, 241
- Marchal, C., & Bozis, G. 1982, *Celestial Mechanics*, 26, 311
- Marcy, G. W., Weiss, L. M., Petigura, E. A., et al. 2014a, ArXiv e-prints, arXiv:1404.2960
- Marcy, G. W., Isaacson, H., Howard, A. W., et al. 2014b, *Astrophys. J. Suppl.*, 210, 20
- Mardling, R. A. 2007, *Monthly Not. Royal Astron. Soc.*, 382, 1768
- Marzari, F., Tricarico, P., & Scholl, H. 2002, *Astrophys. J.*, 579, 905
- Masset, F. S., Morbidelli, A., Crida, A., & Ferreira, J. 2006, *Astrophys. J.*, 642, 478
- Mayor, M., Bonfils, X., Forveille, T., et al. 2009, *Astron. Astrophys.*, 507, 487
- McCarthy, C., & Castillo-Rogez, J. C. 2013, *Planetary Ices Attenuation Properties*, ed. M. S. Gudipati & J. Castillo-Rogez, 183
- McKay, C. P., & Stoker, C. R. 1989, *Reviews of Geophysics*, 27, 189
- Mundy, L. G., Looney, L. W., & Welch, W. J. 2000, *Protostars and Planets IV*, 355
- Murray, C. D., & Dermott, S. F. 1999, *Solar system dynamics*
- Neron de Surgy, O., & Laskar, J. 1997, *A & A*, 318, 975
- Ogihara, M., & Ida, S. 2009, *Astrophys. J.*, 699, 824
- Ohmoto, H., Watanabe, Y., & Kumazawa, K. 2004, *Nature*, 429, 395
- Pierens, A., Cossou, C., & Raymond, S. N. 2013, *Astron. Astrophys.*, 558, A105
- Pierrehumbert, R., & Gaidos, E. 2011, *Astrophys. J. Letters*, 734, L13
- Quintana, E. V., Barclay, T., Raymond, S. N., et al. 2014, *Science*, 767, 128
- Rauer, H., Gebauer, S., von Paris, P., et al. 2011, *Astron. Astrophys.*, 529, A8
- Raymond, S. N., Barnes, R., & Mandell, A. M. 2008, *Monthly Not. Royal Astron. Soc.*, 384, 663
- Raymond, S. N., & Cossou, C. 2014, *Monthly Not. Royal Astron. Soc.*, 440, L11
- Raymond, S. N., Kokubo, E., Morbidelli, A., Morishima, R., & Walsh, K. J. 2013, *Protostars and Planets 6*, in press, arXiv:1312.1689
- Raymond, S. N., O'Brien, D. P., Morbidelli, A., & Kaib, N. A. 2009, *Icarus*, 203, 644
- Raymond, S. N., Quinn, T., & Lunine, J. I. 2005a, *Astrophys. J.*, 632, 670
- . 2005b, *Astrophys. J.*, 632, 670
- Raymond, S. N., Scalo, J., & Meadows, V. S. 2007, *Astrophys. J.*, 669, 606
- Rossow, W. B., & Schiffer, R. A. 1999, *Bull. Americ. Meteor. Soc.*, 80, 2261
- Rothschild, L. J., & Mancinelli, R. L. 2001, *Nature*, 409, 1092
- Sagan, C., Thompson, W. R., Carlson, R., Gurnett, D., & Hord, C. 1993, *Nature*, 365, 715
- Sándor, Z., Süli, Á., Érdi, B., Pilat-Lohinger, E., & Dvorak, R. 2007, *Monthly Not. Royal Astron. Soc.*, 375, 1495
- Schulze-Makuch, D., Méndez, A., Fairén, A. G., et al. 2011, *Astrobiology*, 11, 1041
- Selsis, F., Kasting, J. F., Levrard, B., et al. 2007, *Astron. Astrophys.*, 476, 1373

- Spiegel, D. S., Menou, K., & Scharf, C. A. 2008, *Astrophys. J.*, 681, 1609
- . 2009, *Astrophys. J.*, 691, 596
- Spiegel, D. S., Raymond, S. N., Dressing, C. D., Scharf, C. A., & Mitchell, J. L. 2010, *Astrophys. J.*, 721, 1308
- Stevenson, D. J. 1999, *Nature*, 400, 32
- Terquem, C., & Papaloizou, J. C. B. 2007a, *Astrophys. J.*, 654, 1110
- . 2007b, *Astrophys. J.*, 654, 1110
- Tremaine, S., & Dong, S. 2012, *Astron. J.*, 143, 94
- Turekian, K. K., & Clark, Jr., S. P. 1975, *J. Atmosph. Sciences*, 32, 1257
- Udry, S., Bonfils, X., Delfosse, X., et al. 2007, *Astron. Astrophys.*, 469, L43
- Valencia, D., O'Connell, R. J., & Sasselov, D. 2006, *Icarus*, 181, 545
- von Paris, P., Grenfell, J. L., Rauer, H., & Stock, J. W. 2013, *Planet. Space Science*, 82, 149
- von Paris, P., Gebauer, S., Godolt, M., et al. 2010, *Astron. Astrophys.*, 522, A23
- Walker, J. C. G., Hays, P. B., & Kasting, J. F. 1981, *J. Geophys. Res.*, 86, 9776
- Ward, W. R. 1997, *Icarus*, 126, 261
- Weidenschilling, S. J. 1977, *Ap&SS*, 51, 153
- Weiss, L. M., & Marcy, G. W. 2014, *Astrophys. J. Letters*, 783, L6
- Weiss, L. M., Marcy, G. W., Rowe, J. F., et al. 2013a, *Astrophys. J.*, 768, 14
- . 2013b, *Astrophys. J.*, 768, 14
- Williams, D. M., Kasting, J. F., & Wade, R. A. 1997a, *Nature*, 385, 234
- . 1997b, *Nature*, 385, 234
- Williams, J. P., & Cieza, L. A. 2011, *Ann. Rev. Astron. Astrophys.*, 49, 67
- Wordsworth, R. 2012, *Icarus*, 219, 267
- Wordsworth, R., Forget, F., Selsis, F., et al. 2010, *Astron. Astrophys.*, 522, A22
- Wordsworth, R. D., Forget, F., Selsis, F., et al. 2011, *Astrophys. J. Letters*, 733, L48
- Yang, J., Cowan, N. B., & Abbot, D. S. 2013, *Astrophys. J. Letters*, 771, L45